

Design of a High-Speed Signal Processing System for Underwater LiDAR Based on Complete Waveform Sampling [†]

Guangbo Xu

School of Mechanical Engineering, Nanjing University of Science and Technology, Nanjing 210094, China; xgbxgb@njust.edu.cn; Tel.: +86-25-84315455

[†] Presented at the 4th International Electronic Conference on Applied Sciences, 27 October–10 November 2023; Available online: <https://asec2023.sciforum.net/>.

Abstract: The complex and changing underwater environment, along with the presence of various suspended particles, leads to laser attenuation and backward scattering. As a result, the detection capabilities of underwater LiDAR are significantly limited. To address the challenges associated with the backward scattering problem using traditional time discrimination circuits, this paper proposes a high-speed signal processing system for underwater LiDAR based on complete waveform sampling. The system includes the design of a photodiode preamplifier circuit and a main control board with a sampling frequency of up to 2 GHz. With this design, the underwater LiDAR can achieve a ranging accuracy of 0.075 m and implement relevant backscatter filtering algorithms. This paper can serve as a valuable reference for the design of signal processing systems for underwater LiDAR.

Keywords: LiDAR; underwater laser detection; FPGA

1. Introduction

LIDAR has been widely used in target ranging and target imaging studies due to its advantages of high accuracy and high resolution [1–6]. Its target detection in the air has been extensively studied and validated. Currently, the main ranging method of LiDAR in the air is the time-of-flight (TOF) method, which measures the time elapsed from the laser emission (start signal) to the laser reflected back from the target (stop signal), and then calculates the target distance based on the known speed of light. A major step in the process is to convert the electrical signal received by the photodiode into a stop signal to stop the timing in the TDC chip—called time discrimination. The traditional method of time discrimination is to judge the laser return signal through a comparator that exceeds a certain threshold. This method is called the threshold method [7,8].

Despite the presence of a transmissive window for lasers underwater, seawater and impurities in seawater can cause strong backscattering of the laser light. This phenomenon results in the underwater LIDAR receiving a strong backscattered signal, regardless of whether it detects the target or not. This can lead to misjudgment or omission of the LIDAR, rendering the traditional time discrimination method ineffective.

In this paper, a high-speed signal processing system based on full waveform sampling is proposed for underwater LiDAR. The system has a sampling frequency of up to 2 GHz, allowing it to convert the typical laser echo signal into hundreds of discrete data points. Then, the backward scattering algorithm is utilized to filter out the backward scattering component and extract the target echo signal. Subsequently, the traditional time discrimination method can be employed to obtain the accurate echo time. The high-speed signal processing system for underwater LiDAR proposed in this paper can serve as a reference for the hardware design of underwater LiDAR, ensuring both ranging accuracy and signal processing capability.

Citation: Xu, G. Design of a High-Speed Signal Processing System for Underwater LiDAR Based on Complete Waveform Sampling. *Eng. Proc.* **2023**, *52*, x. <https://doi.org/10.3390/xxxxx>

Academic Editor: Andrea Ballo

Published: date



Copyright: © 2023 by the author. Submitted for possible open access publication under the terms and conditions of the Creative Commons Attribution (CC BY) license (<https://creativecommons.org/licenses/by/4.0/>).

2. Underwater LiDAR TOF Ranging Method Based on Complete Waveform Sampling

As shown in Figure 1, underwater laser detection is different from atmospheric laser detection. Due to the scattering and absorption effect of the water for the light, the acquisition of the target echo signal is seriously disturbed. When the light pulse signal is transmitted in the water, the photons will interact with water molecules and suspended particles so that the photon transmission direction is randomized, and part of the light energy before reaching the detection target is reflected by the water causing the backscattered signal (as shown in the Figure 1 of the backscattered echo peak); another part of the signal reflected by the target back to the detector receiving surface is affected by the forward scattering and water absorption properties of light. So, the target echo signal will be broadened.

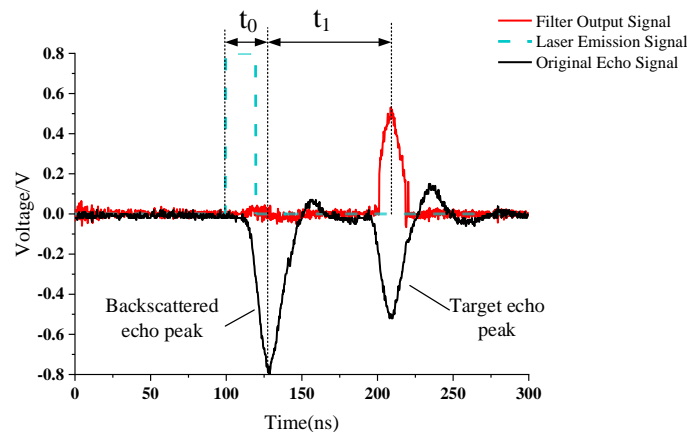


Figure 1. The block diagram of the TOF ranging principle of underwater LiDAR based on complete waveform sampling.

The ranging accuracy of the LiDAR is linearly related to the time measurement accuracy, i.e., the accuracy of the laser flight time T measurement directly affects the measurement accuracy of the distance R . As shown in the black curve in Figure 1, if the peak moment discrimination circuit in the traditional LiDAR is used, the measured laser flight time is t_0 . In contrast, the actual laser flight time is $t_0 + t_1$, with a sizeable ranging error.

3. High-Speed Data Processing System Hardware Design and Experimental Verification

Due to the narrow pulse width of the laser pulse echo signal, a sampling frequency of 2G Hz is used to sample the entire waveform of the laser pulse echo signal to make the sampled signal not distorted and to meet the ranging accuracy of the LiDAR.

The specific workflow of the high-speed data acquisition system is as follows: the FPGA controls the laser power supply and the high-voltage power supply of the Avalanche Photodiodes (APD) to turn on. It also sends a TTL trigger signal to the laser and the high-speed data acquisition system making the laser send out a pulsed laser beam. In the meantime, the high-speed data acquisition system samples the entire waveform of the APD's echo signal and processes it with algorithms such as backward scattering filtering, low-pass filtering, peak finding, and moment discrimination. Subsequently, the sampling point number between the laser transmitting point and the laser receiving point is calculated and multiplied by the sampling interval of the high-speed data acquisition system to obtain the time interval value, which can be converted into the distance value.

The design adopts the direct sampling method to acquire the entire waveform of the laser pulse echo signal, and the block diagram of the high-speed data acquisition system is shown below. It mainly consists of an analog conditioning circuit, a high-speed AD sampling chip, a high-precision clock tree chip, and a Central Process Unit.

The analog conditioning circuit is responsible for converting the current signals captured by the APD into voltage signals that can be recognized by the AD converter. The AD converter, in turn, is responsible for converting the laser echo signals into data points that can be processed. The CPU handles the provision of peripheral interfaces and data processing. Lastly, the clock tree provides a fast and synchronized clock for the high-speed AD converter and the CPU.

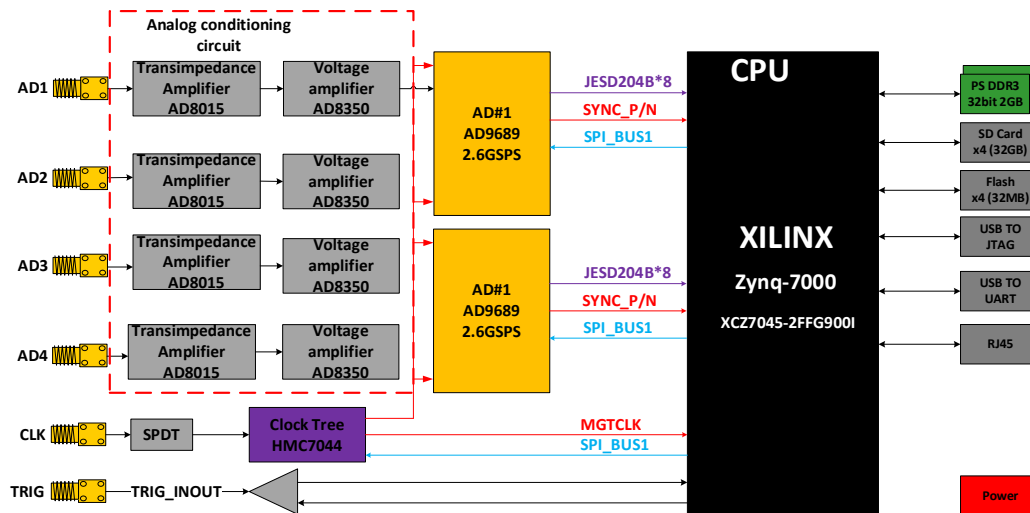


Figure 2. The block diagram of the high-speed data acquisition system.

3.1. Analog Conditioning Circuit

Due to the laser pulse echo signal’s narrow pulse width, a sampling frequency of 2 GHz is employed to ensure the entire waveform is accurately sampled without distortion. It is important that this method can also meet the LiDAR’s ranging accuracy requirements.

Since the current signal-to-noise ratio of the APD output is small and the signal amplitude, etc., cannot meet the processing requirements of the subsequent circuit, an amplifier is required to amplify its output signal. The purpose of the trans-impedance amplifier is to amplify the weak signal and convert the current signal into a voltage signal, so the primary consideration for the trans-impedance amplifier is the bandwidth and gain, i.e., the gain-bandwidth product. The bandwidth of the selected trans-impedance amplifier should be related to the rising edge time of the converted signal from the APD, which is 2 ns, so the bandwidth of the trans-impedance amplifier can be calculated using the empirical formula, which is about 175 MHz. Therefore, the bandwidth of the selected circuit should be bigger than 175 MHz.

Because the input signal is a broadband signal, so need to choose a broadband amplifier; Secondly, the trans-impedance amplifier requires a single power supply to simplify the circuit design; In addition, the trans-impedance amplifier also needs to have low noise characteristics, such as a broadband trans-impedance amplifier can be designed with operational amplifiers to meet the indicators, but also can be achieved with a unique trans-impedance amplifier. Currently, the amplifiers that can meet the above requirements are mainly TI’s operational amplifiers OPA354, OPA656, OPA857, and ADI’s trans-impedance amplifier AD8015, whose leading indicators are shown in the table below.

Table 1. Main specifications of the trans-impedance amplifier on the market.

Model	Whether It Is Differential Output	Bandwidth	Operating Voltage
OPA345	N	100 MHz	2.5–5.5 V
OPA656	N	500 MHz	5 V
OPA857	N	125 MHz	2.7–3.6 V
AD8015	Y	240 MHz	5 V

TI’s amplifiers are mainly general-purpose amplifiers, i.e., trans-impedance amplifiers with external resistors in the operational amplifier. ADI’s trans-impedance amplifier is characterized by its built-in resistors, constant gain, and differential amplifiers. Due to the limited size of the board, the final system is a laminated structure, which may generate interference within the system. The advantage of differential amplifiers is that they can effectively suppress interference from outside and from the system itself. The AD8015 is chosen as the trans-impedance amplifier after comparison.

The AD8015 is a low-noise single-ended differential output amplifier with a built-in constant gain of 20 K, a bandwidth 240 MHz, an output impedance of 50 ohms, and a dynamic range of 17 dB. Given this situation, this paper adopts the method of differential transmission and differential amplification to reduce the crosstalk between channels effectively.

The current of the echo signal from the APD to 60 nA. The output voltage resulting from this current passing through the trans-impedance amplifier should be 1.2 mV. Figure 3 displays the circuit diagram of the trans-impedance amplifier as designed.

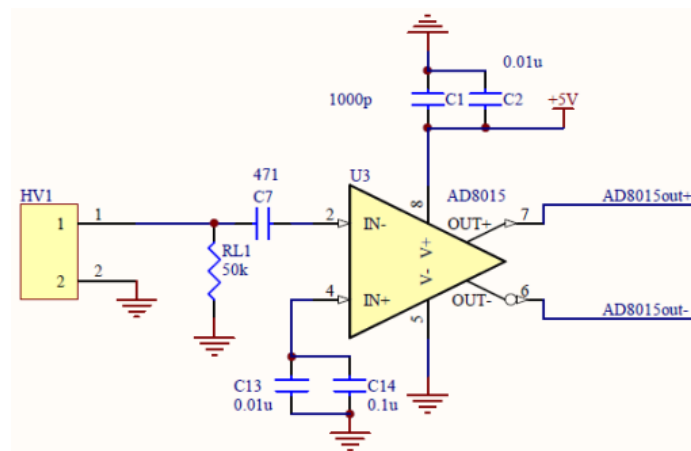


Figure 3. The diagram of the AD8015.

After the trans-impedance amplifier, the current signal from the APD detector still cannot meet the requirements, so after the trans-impedance amplifier, another voltage amplifier is needed to amplify the return signal. After the trans-impedance and voltage amplifiers, the signal needs to be recognized for subsequent processing. Since the current signal from the APD has been amplified into a voltage signal by the trans-impedance amplifier, the following amplification circuit should use a voltage amplifier.

The AD8350 is an amplifier with low noise, high gain, and differential input and output, which meets this paper’s requirements of crosstalk reduction. Figure 4 shows the circuit diagram of the designed voltage amplifier.

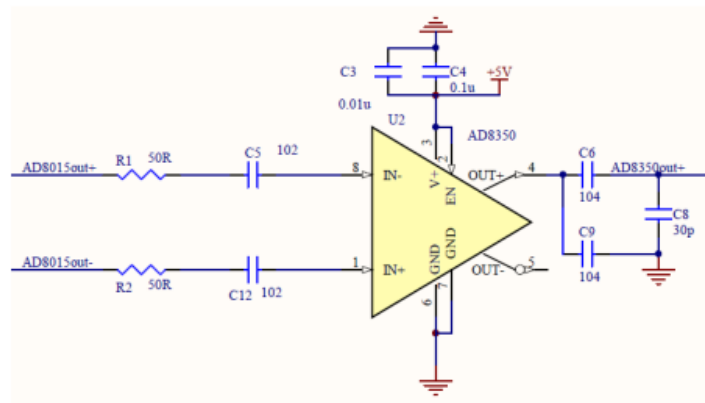


Figure 4. The diagram of the AD8350-15.

3.2. High-Speed Data Acquisition Test

The high-speed data acquisition test is conducted using a range of equipment such as a high-speed data acquisition board, upper computer, oscilloscope, DC power supply, target board, and laser emission and reception test box. During the test, the laser emission and reception test box irradiates the target board, while both the oscilloscope and high-speed data acquisition board simultaneously collect the resulting laser echo signal.

The test results, depicted in the figure below, indicate that there is no waveform distortion between the data captured by the high-speed data acquisition system and the waveform monitored by the oscilloscope via the computer. As a result, the test was deemed successful.

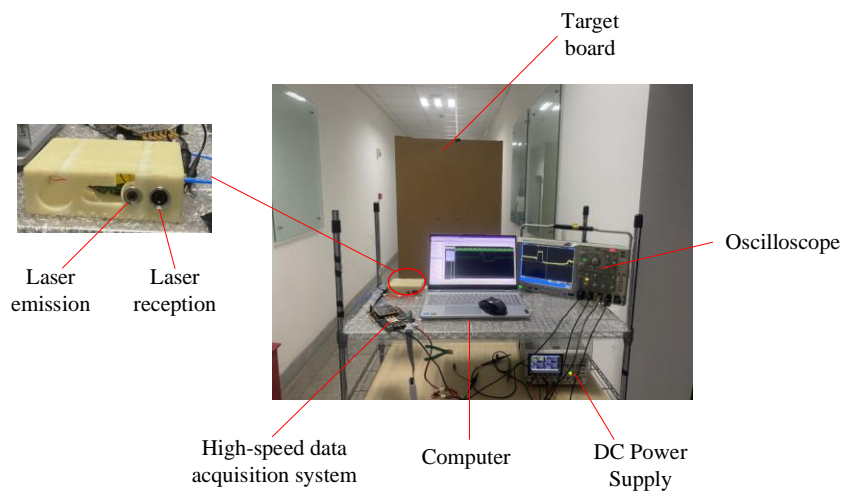


Figure 5. The diagram of the test scene.

4. Conclusions

In this paper, an underwater LiDAR high-speed signal processing system is proposed based on full-waveform sampling. The system consists of a front-end analog conditioning circuit that converts the current signals acquired by the avalanche photodiode (APD) into voltage signals compatible with the analog-to-digital (AD) chip. Additionally, the Xilinx Zynq-7000 series is utilized as the peripheral interface and data processing chip for the system. The proposed system achieves a sampling frequency of up to 2 GHz and a ranging accuracy of 0.075 m. It is capable of implementing various signal processing algorithms, including the backscatter filtering algorithm.

Funding: This work is supported by the 2021 Open Project Fund of Science and Technology on Electromechanical Dynamic Control Laboratory, grant number 212-C-J-F-QT-2022-0020; Post-graduate Research & Practice Innovation Program of Jiangsu Province, grant number KYCX23_0511.

Acknowledgments: The authors would like to thank the peer reviewers and editors for their hard work and constructive feedback, which will make a significant contribution to improving the paper.

Conflicts of Interest: The authors declare that they have no known competing financial interests or personal relationships that could have appeared to influence the work reported in this paper.

References

1. Zheng, Z.; Zha, B.; Zhou, Y.; Huang, J.; Xuchen, Y.; Zhang, H. Single-Stage Adaptive Multi-Scale Point Cloud Noise Filtering Algorithm Based on Feature Information. *Remote Sens.* **2022**, *14*, 367. <https://doi.org/10.3390/rs14020367>.
2. Zheng, Z.; Zha, B.; Xu, C. Adaptive edge detection algorithm based on improved grey prediction Model. *IEEE Access* **2020**, *8*, 102165–102176.
3. Tan, Y.; Zhang, H.; Zha, B. Underwater single beam circumferentially scanning detection system using range-gated receiver and adaptive filter. *J. Mod. Opt.* **2017**, *64*, 1648–1656.
4. Xu, C.; Zha, B.; Bao, J. Analysis of temporal and spatial distribution characteristics of ammonium chloride smoke particles in confined spaces. *Def. Technol.* **2022**, *18*, 1269–1280.
5. Xu, C.; Zhang, H.; Zha, B. Numerical Simulation of Dust Concentration Distribution in Confined Space. *Acta Armamentarii* **2020**, *41*, 618–624.
6. Xu, G.; Zha, B.; Xia, T.; Zheng, Z.; Zhang, H. A High-Throughput Vernier Time-to-Digital Converter on FPGAs with Improved Resolution Using a Bi-Time Interpolation Scheme. *Appl. Sci.* **2022**, *12*, 7674. <https://doi.org/10.3390/app12157674>.
7. Xu, G.; Zha, B.; Zheng, Z.; Zhang, H. Design and Modeling of Small-Opening Cascade Synchronous Scanning Underwater LiDARs. *Acta Armamentarii* **2022**, *43*, 3162–3171.
8. Xu, G.; Zha, B.; Yuan, H.; Zheng, Z.; Zhang, H. Underwater four-quadrant dual-beam circumferential scanning LiDAR using nonlinear adaptive backscatter filter based on pauseable SAF-LMS algorithm. *Defence Technol.* **2023**, <https://doi.org/10.1016/j.dt.2023.06.011>.

Disclaimer/Publisher's Note: The statements, opinions and data contained in all publications are solely those of the individual author(s) and contributor(s) and not of MDPI and/or the editor(s). MDPI and/or the editor(s) disclaim responsibility for any injury to people or property resulting from any ideas, methods, instructions or products referred to in the content.